Earthshine and the Earth's Albedo

A [1,2], B[2], C[3] and D[3]

[1] U1

[2] U2

[3] U3

Received ______________; accepted ______________

ABSTRACT

Earthshine

Subject headings: Earth: albedo, global climate — Moon: reflection

1. Introduction

The earth's climate depends on the net sunlight deposited in the terrestrial atmosphere, which is critically sensitive to the earth's albedo. Thus, the earth's energy balance is determined in large part by its albedo−−the fraction of the incident sunlight that is directly reflected back into space without altering the internal energy budget of the atmosphere. The earth's surface, aerosols in the atmosphere, and clouds all reflect some of the incoming solar short-wavelength radiation, preventing that energy from warming the planet. Short-wavelength radiation, usually defined as having wavelengths between 0.15 and 4.0 μm, includes about 99% of the Sun's radiation; of this energy, 46% is infrared (> 0.74 μm), 9% is ultraviolet (< 0.4 μm) and the remaining 45% is visible, with wavelengths between 0.4 and 0.74μm. A significant portion of the solar energy is absorbed by the earth, where it drives terrestrial phenomena before being radiated back into space. This long-wavelength radiation peaks at about 15 μm (corresponding to a black-body temperature of about $T_E = 255$ K).

A global albedo can be determined by measuring the amount of sunlight reflected from the earth and, in turn, back to the earth from the dark portion of the face of the Moon (the "earthshine" or "ashen light"). The most important historical program of earthshine measurements was carried out by Danjon (1928, 1954) from a number of sites in France. He used a "cat's-eye" photometer to produce a double image of the Moon, allowing the visual comparison of the intensities of two well-defined patches of the lunar surface−−one in sunlight and the other in the earthshine−−at various lunar phases. Using the "cat's-eye" mechanism, he stopped down the light from the sunlit portion to match the brightness of the ashen portion. This differential measurement removed many of the uncertainties associated with varying atmospheric absorption and the solar constant, allowing Danjon to achieve an estimated uncertainty of roughly 5%. Our measurements are much more precise not simply because we have better cameras available, but we have also solved the problem of the uncertainty in the scattering from the moon as a function of the phase of the moon (see §6).

From 1926 to 1930, Danjon made 207 measurements of earthshine. Dubois (1947) continued the program through 1960 from the observatory at Bordeaux using a Danjon-type photometer.

Danjon's and Dubois' results show a number of interesting features. The daily mean values of the observations vary more widely than would be expected on the basis of the variation of measurements on a single night. This can be plausibly attributed to daily changes in cloud cover, but extensive cloud-cover data were not available at the time of the observations.

Danjon (1928) also examined his observations to determine whether there was a long-term trend in albedo, but found none. Dubois' observations for some 20 years ending in 1960 showed considerable annual variability, which he speculated was due to solar activity. His published monthly variations from 1940-1944 also show a strong correlation with the 1941-42 El Nino. In the past forty years, there have been some observations of earthshine by Huffman et al. (1989) and one-time observations by Franklin (1967) and Kennedy (1969).

The observations reported here were carried out at Big Bear Solar Observatory (BBSO) beginning December , using our earthshine telescope. The observations are described in detail in §3. We note that our CCD detector has sufficient resolution and dynamic range to observe both the sunlit and earthshine portions of the Moon in the same image (although a dark filter is usually interposed on the bright crescent), so the entire disk is measured at once. We report the results of our data including synoptic, seasonal, and annual variability.

We also compare the results from our observations with the first modern modeling of earthshine. These calculations used ERBE scene models, a general circulation model (GCM) derived snow/ice covers to simulate both earthshine and input cloud cover data from operating meterological satellites which are contemporaneous to the observations to which they are compared (see §9).

2. Determining the Earth's Albedo from Earthshine

Terrestrial measurements of the short-wavelength (visible light and near infrared) albedo of a planet in our solar system is relatively straightforward – except for the earth. However, we can determine the albedo from the ground by measuring the earthshine. From a terrestrial perspective, the earthshine is the sunlight reflected from the bright side of the earth to the moon and finally back to an observer on the dark side of the earth. To begin, we consider the ratio of the earthlight to sunlight, Γ, that would be seen by an observer on the moon. There is a systematic variation of Γ throughout the lunar month. When the moon is nearly new (lunar phase $\theta \approx \pm\pi$), the earth is nearly full, and so Γ is relatively large ($\approx 10^{-4}$). Conversely, when the moon is nearly full ($\theta \approx 0$), the earth is a thin cresent and Γ becomes vanishingly small. Fluctuations of Γ about its average behavior are caused by varying terrestrial conditions, including weather, the seasons and climate change. The lunar phase, θ is defined in Figure 1.

In terms of the reflectance properties of the earth,

$$\Gamma = \frac{1}{\pi R_{em}^2}[\frac{R_{ms}}{R_{es}}]^2 \int_{(\hat{R}\cdot\hat{S},\hat{R}\cdot\hat{M})\geq 0} d^2R(\hat{R}\cdot\hat{S})a(\hat{R}\cdot\hat{M}), \tag{1}$$

where d^2R is an element of the earth's surface, $\hat{R}$ is a unit vector pointing toward the local zenith and $\hat{S}$ is a unit vector pointing toward the sun, and where R_{em}, R_{ms} and R_{es} are the earth-moon, moon-sun and earth-sun distances, respectively. $\hat{M}$ is the unit vector pointing from the earth toward the moon, and the integral is over all of the earth's surface for which the sun and moon are simultaneously above the horizon (i.e., $\hat{R}\cdot\hat{S}$ and $\hat{R}\cdot\hat{M} \geq 0$). The albedo of each surface element, a_e, depends on the surface type, cloud and snow/ice cover and solar zenith angle.

The evaluation of equation (1) would be straightforward if the earth were a Lambert sphere, i.e., if it were to reflect isotropically from its assumed to be fully diffusive surface. If so, the lunar observer would measure

$$\Gamma_L = \frac{2}{3}\frac{a_L f_L(\alpha) R_e^2}{R_{em}^2}[\frac{R_{ms}}{R_{es}}]^2, \tag{2}$$

where R_e is the earth's radius, α is the earth's phase (see Figure 1) and f_L, the *earth's* Lambert phase function, is determined by

$$f_L(\alpha) = \frac{(\pi-\alpha)\cos\alpha + \sin\alpha}{\pi}. \tag{3}$$

The earth's phase function is very roughly Lambertian for $\alpha \geq \frac{2\pi}{3}$ (see §7).

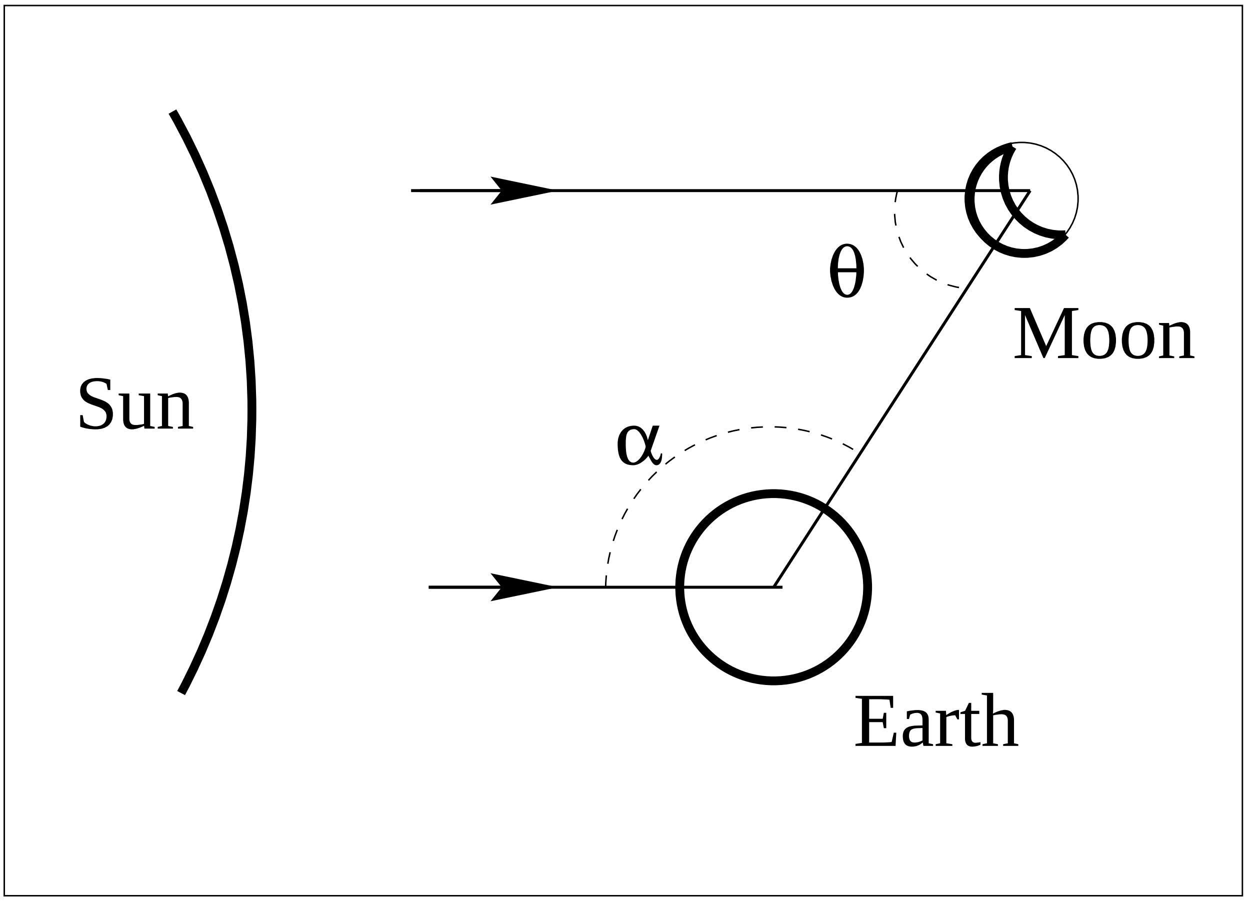

Fig. 1.— A sketch of the sun-earth-moon system defining the earth's phase angle, α, and moon's phase angle, θ.

Essentially, the lunar observer sees an instantaneous, differential cross section of the sunlight reflected from the earth. The differential cross section depends on the earth's geometrical albedo and the phase of the moon. At the earth's surface, the differential cross-section of the reflected sunlight for scattering by an angle α (note that α is the supplement of the usual scattering angle) is given by

$$\frac{d\sigma}{d\Omega} \equiv p_e f_e(\alpha) R_e^2, \tag{4}$$

where p_e is the geometrical albedo of the earth arising from the individual a_e and f_e is the earth's phase function, defined such that $f_e(0) = 1$, as can be seen in the Lambertian limit from equation (3).

The formulation in equation (4) is separable, so that we can write the total scattering cross section as

$$\sigma = \int \frac{d\sigma}{d\Omega} d\Omega = \pi R_e^2 p_e \int_{-\pi}^{\pi} f_e \mid \sin(\alpha) \mid d\alpha, \tag{5}$$

where p_e depends on the earth's weather, season and climate, while f_e depends on the earth's aspect. In practice, we integrate over the phases of the moon to determine the total cross section.

From the total cross section, we can define the Bond albedo, the fraction of solar energy incident on the planet that is reflected, as

$$A_B = \frac{\sigma}{\pi R_e^2} = 2p_e \int_0^{\pi} f(\alpha)\sin(\alpha) d\alpha. \tag{6}$$

If we assume that the earth is a Lambert sphere, we can do the integral exactly asuming the earth's phase function is given by equation (3), then we determine a simple proportionality between the geometric albedo and the global or Bond albedo, namely,

$$p_{e,L} = \frac{2}{3} A_{B,L}. \tag{7}$$

Again, modeling discussed in §7 shows that the earth's phase function is approximately Lambertian for $\alpha < \frac{2\pi}{3}$. Thus, a convenient, differential measure of the earth's reflectivity is the effective albedo

$$A^* = \frac{3}{2} \frac{p_e f_e}{f_L}. \tag{8}$$

which is the albedo of a Lambert sphere that would give the same instantaneous reflectivity as the true earth.

At that instant, the observer on the moon in the region illuminated by the sun and visible from the earth would see both the direct sunlight and some part of the sunlit earth. The solar intensity seen by that observer would be

$$I_e = \frac{C_s}{R_{ms}^2}, \tag{9}$$

where C_s is the solar constant and R_{ms} is measured in astronomical units. Similarly, the intensity of the earthlight would be

$$I_e = \frac{C_s}{R_{es}^2} p_e f_e(\alpha) \frac{R_e^2}{R_{em}^2}. \tag{10}$$

Thus, the earth's reflectivity can be expressed as

$$p_e f_e = \frac{I_e}{I_s}[\frac{R_{em}}{R_e}]^2. \tag{11}$$

In the observations, we study two diametrically opposite fiducial patches both near the night time lunar limb. For our purposes here, we call them "a" and "b" and treat them as unit projected areas. If a is illuminated only by the earthshine, the intensity observed by an observer on the earth at a distance R_{oa} would be

$$I_a = I_e \frac{p_a f_a(0)}{R_{oa}^2} T_a, \tag{12}$$

where T_a is the transmission of the earthshine through the atmosphere, and $f_a(0)$ is the *lunar* phase function for the retroflection from patch a. We note that the expression for the lunar Lambert phase function is the same as given in equation (3) with α replaced by θ. Similar to equation (12), the intensity of the sunlit portion, b, would be

$$I_b = I_e \frac{p_b f_b(\theta)}{R_{ob}^2} T_b, \tag{13}$$

where the lunar phase function, $f_b(\theta)$ embodies the dependence of the fiducial patch on the angle between the sunlight reflected off the moon (so-called "moonshine") to the terrestrial observer, again see Figure 1. Thus,

$$\frac{I_a}{I_b} = \frac{I_e}{I_s} \frac{1}{f_b(\theta)} \frac{R_{ob}^2}{R_{oa}^2} \frac{T_a}{T_b}, \tag{14}$$

and so

$$p_e f_e = \frac{I_a}{I_b} f_b(\theta) [\frac{R_{em}}{R_e}]^2 \frac{T_b}{T_a} \frac{p_b}{p_a} [\frac{R_{oa}}{R_{ob}}]^2 [\frac{R_{es}}{R_{ms}}]^2. \tag{15}$$

Since $\frac{R_{em}}{R_{es}} \sim 5 \times 10^{-3}$, we can safely set the the last factor in equation (15) to unity. Similarly, we can set the second to last factor to unity. Further, we can also safely set $\frac{T_a}{T_b}$ to unity because site surveys at BBSO have shown a close correlation between atmospheric turbulence over several tens of meters and that the seeing arised fairly close to the ground, Goode, et al. (1999). Thus, we determine that

$$p_e f_e = \frac{I_a}{I_b} f_b(\theta) [\frac{R_{em}}{R_e}]^2 \frac{p_b}{p_a}. \tag{16}$$

We measure I_a and I_b in our nightly observations. We have measured the lunar phase function quite accurately over the last year. We need a total eclipse to measure $\frac{p_b}{p_a}$,

3. Observations: Earthshine Instrumentation and Data Acquisition

Earthshine observations are currently being carried out at BBSO. The earthshine telescope is mounted atop the 65 cm solar telescope.

3.1. Hardware

The basic optical components of the earthshine telescope consist of an f/15 telescope primary with a 6-inch diameter air spaced doublet. The telescope tube is attached and aligned with the 65 cm solar telescope which enables us to use the large telescope's drive software – permitting tracking following the moon's variable rate. At the end of the tube is a stray light field stop. The incoming moonlight passes the field stop, and then enters a light tight optical assembly box that holds the filters and camera optics.

In the box, just behind the tube field stop and just before prime focus, is the earthshine neutral density filter switcher. Two filters are placed in the switcher. The first neutral density filter is a Schott NG3 2mm (transmission 0.0117 from 4000-7000 Å) for the Bright Side (BS) measurements. The second filter is a Schott NG10 2mm (transmission is about 2×10^{-5} 4000-6000Å) which is essentially a blocking filter to cutoff the bright side of the moon to permit the dark side or earthshine (ES) observations. The BS filter covers the entire field of view and is in place to prevent camera saturation and to provide a reasonable exposure range. The ES filter is covers the bright side of the moon to permit long, dark side exposures to get optimal signal to noise for the ES images. The ES filter is carefully placed within the switcher filter holder, by hand, at the beginning of each observing session. It location, designed to cover the terminator, depends on the phase and libration of the moon. Both filters were scanned to check transmission with wavelength at Gamma Scientific in San Diego using a Radoma spectroradiometer. Both filters were found to be well within the quoted Schott tolerances.

The prime focus is after the switcher, and it is closely followed by a flat field lens. Next in the optical train are two near IR filters that stop any light beyond 7000 Å from reaching the camera.

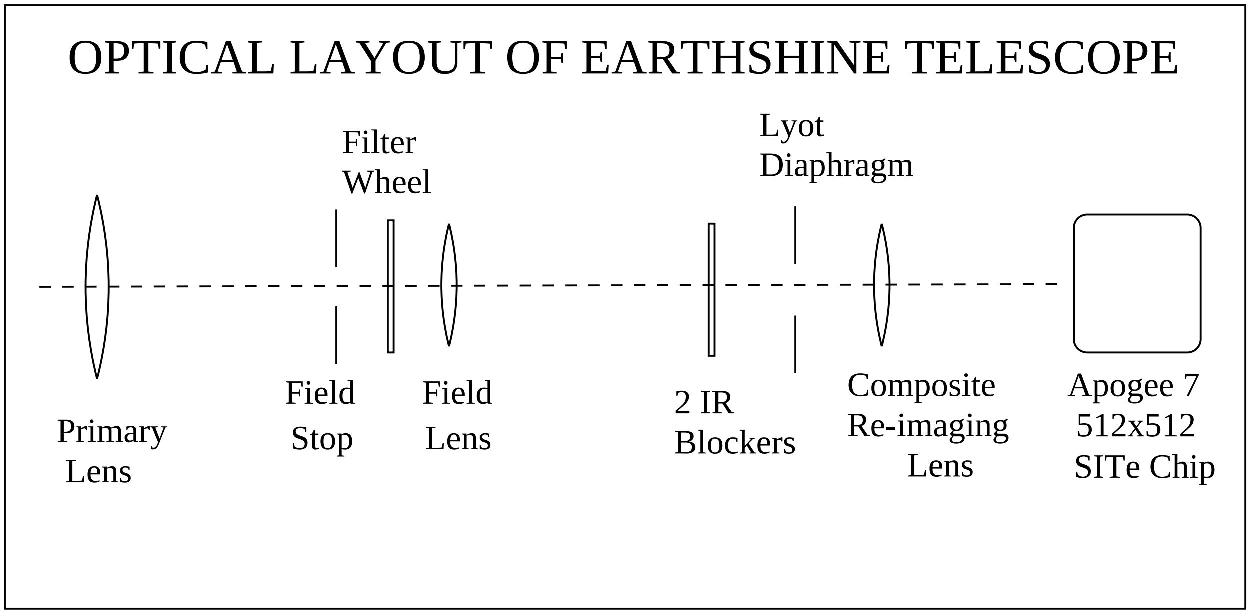

Fig. 2.— The optical set-up of the earthshine telescope.

An iris behind the near IR filters acts as a further stray light stop. Behind the iris is a camera lens that focuses the lunar image on the CCD. Between this lens and the camera is a space for a filter wheel which can be used for narrow band measurements. All elements are rail mounted for linear adjustments, and lens elements are in moveable $y - z$ mountings for fine adjustments. All fine-tuning was in the Fall of 1998, and nothing has been changed on the system since the start of data acquisition in December 1998. The system was "frozen" to limit possible errors in calibrating the lunar phase function. Flat field images help to point out the location of occasional dust particles that get into the optics. Compressed air removes most particles, and when necessary, elements are removed for cleaning, and then are carefully replaced to preserve optical alignment.

The CCD camera used in our current earthshine observations is an Apogee 7. The camera is a 512 X 512 16-bit scientific system with a SITe back-illuminated, thinned silicon chip. This chip, which of SITe's highest grade, is designed for higher quantum efficiency than unthinned front illuminated chips – this advantage is most apparent toward the blue. One drawback of the higher efficiency SITe chip is its' sensitivity to "after-images" caused by exposure to UV. Testing the earthshine system to limit this effect resulted in the following observing procedures: The UV from the BS images is blocked by the NG3 filter. The worst after-images show up in the ES images on the unfiltered half of the image – which are of long exposure. It was found that by increasing the number of short BS images, the UV residual image was removed. Careful examination of dark current and flat field images taken during the course of observations are done to confirm this, night by night.

Initial testing demonstrated a linear response over the camera's entire 16-bit range. To check for change in the camera's response with time, a calibrated radiometer was purchased to check the camera's responsivity during the each new moon. Dome flats are taken in varying illumination to get pixel count versus intensity. The radiometer is an IL 1700, a NIST traceable Silicon photodiode radiometer. Once a year, the radiometer will be returned to International Light for re-calibration.

3.2. Observations

After initial tests, our current round of earthshine observations began in December 1998. The camera's graphic user interface C code, supplied by the manufacturer, was modified to efficiently handle the routine earthshine observations. The nightly observations follow a simple set of procedures. Most are almost completely automated. To begin, a few initial images are taken to center the moon. When the image is centered, the ES filter is set by hand, and the observer retires downstairs to the control room. Then, more images are taken to determine the ES and BS exposures which optimize the signal to noise ratio. Finally, data are taken and stored. During the course of observations BS, ES, dark current, and flat field images are taken, regularly.

The first 8 months of observations covered lunar phases between +140 and -140 degrees, which is about 21 days a month. The initial observation over this wide range of phases was necessary to determine the lunar phase function and prove its' repeatability. During the first 8 months, for the phases near the full moon (+40 through 0 to -40), ES images were not taken because both fiducial patches were in, or so near to sunlight that ES measurements were unreliable. On these nights only BS, dark current, and flat fields, were taken to determine the scattering of light from the fiducial patches as a function of the phase of the moon. The lunar phase function was determined by July 1999, so that the BS only nights were dropped – except for observations of the full moon. Full moon observations are still undertaken to determine the role of the opposition effect (REFERENCE) in the lunar phase function (phases -4° to +4°). Weather willing, the January 2000 total lunar eclipse will allow us to get scattering data very close to zero lunar phase. Current earthshine observations cover about 14 days per month, and cover lunar phases between +/-40 to +/-150 degrees centered about the first and last quarters of the moon, when we have optimal conditions for measuring the earthshine – close to full-earth with a few hours of observations being possible. Data rates vary depending on phase. An average night will give about 1 image per minute. This means that the number of raw images saved, for data reduction, varies between 100 to 600 per night.

4. Data Reduction

4.1. Image Analysis

The earthshine and moonshine intensities are measured by integrating the brightness of each of two physically fixed fiducial patches – one from the bright side and the other from the dark side of the lunar disk. We always use the same two fiducial patches, and for them it is essential to determine the transformation between the CCD image coordinate system and the selenographic (lunar) coordinate system.

For this purpose, we first need to define the limb and center of the lunar disk for each image. Each of the raw lunar images is contrast-enhanced and the limb points are defined by looking for suitable positions of large intensity gradient. Empirically, a minimum of 40 rim points should be obtained, which are then used to make a Maximum Likelihood fitting to decide the lunar center in the image plane. Once the lunar center and limb are determined, the radius of the lunar disk can be easily calculated in the CCD coordinates.

The next step is to find the position of the lunar pole in the image plane. To this end, some outstanding lunar features, whose precise selenographic coordinates are known, are used to co-register the two coordinate systems. The topocentric location of the lunar pole at any given moment can be precisely calculated using parameters from an astronomical almanac, from which, one can determine the projected positions of these lunar features in the image plane which is perpendicular to the vector pointing from the local observer to the lunar center. By comparing these projected positions with the positions of these features in the CCD coordinates, the angle between the projected N-S axis of the moon and the Y-axis of the CCD coordinate system is derived.

Once we have obtained the transformation between the selenographic system and the CCD coordinates system, we are able to locate the fiducial patches in every image of the lunar disk taken in the observations. Particularly, in our study, we decided that the optimum choice for the two fiducial patches is one centered at (-11.2, -71.5) in the Crisium side and the other at (28.5, 72.5) in the Grimaldi side, respectively (the coordinates are in the selenographic system), each covering a longitudinal range of about 10 degrees and latitudinal range of 3 degrees. The patches are both located in the "highlands" of the lunar surface, and the physical reflectivity of the two are roughly comparable. The patch on the Grimaldi side is close to Danjon's choice. While the other patch in our observations is to the south-east of Danjon's patch by about $200''$. Our patch is closer to the limb. The apparent areas of these patches change from night to night because of lunar libration. The intensity is read out as an average of the whole area, and the difference due to the geometric effect of the reflectivity, because of libration, is accounted for in our next step of data analysis (§4.2).

For accurate photometry, flatfielding and dark current subtraction are applied to each image. For earthshine images, we also need to subtract the background scattering from the bright side of the moon. For lunar phase greater than 90 degrees, the background intensity can be regarded as falling off linearly with the distance from the center of the crescent, and the amount of background over the earthshine is extrapolated from a fit of the background just outside the disk's radius.

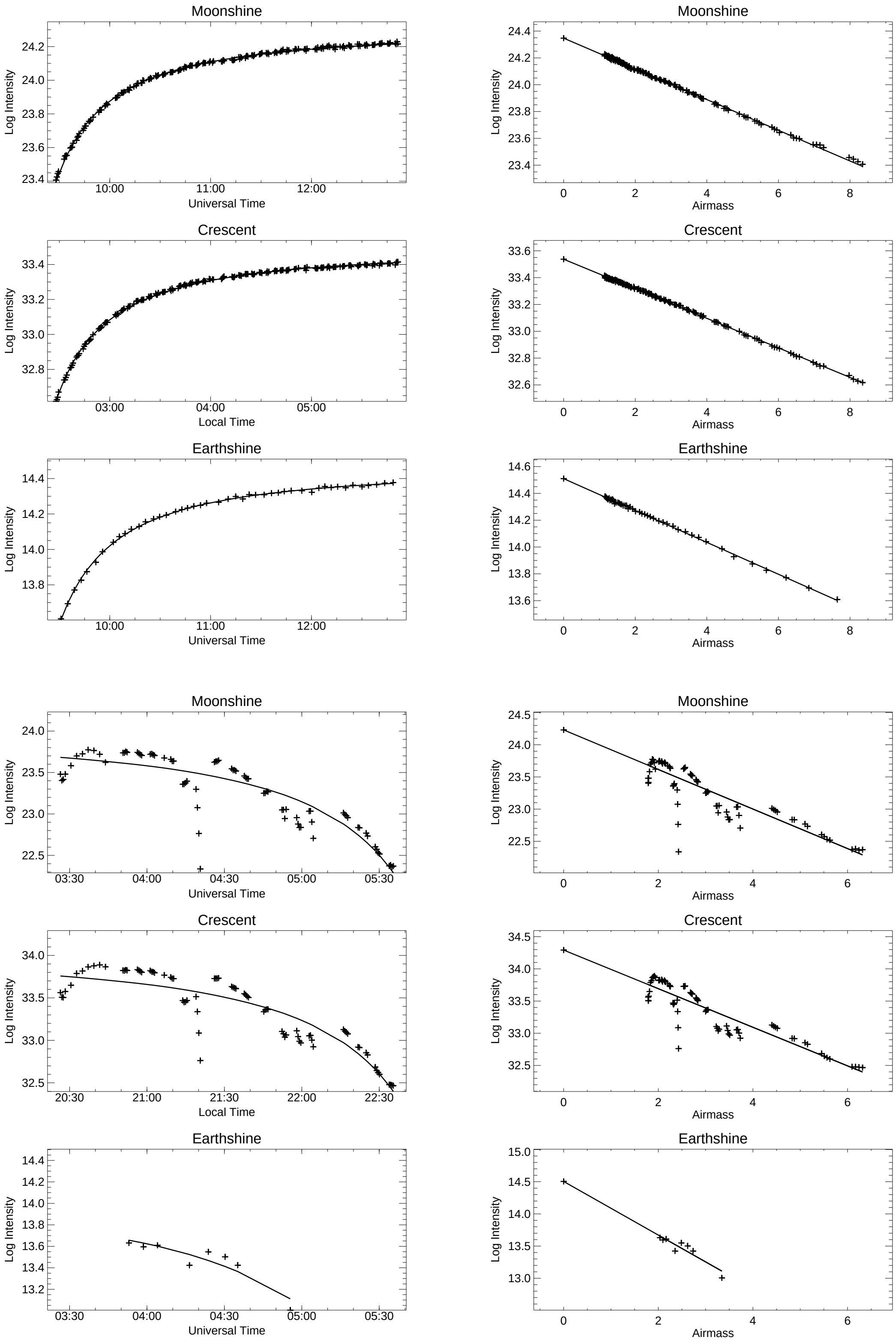

Fig. 3.— In each sub-frame, the moonshine (top panel), crescent (middle panel) and earthshine (bottom panel) intensity is plottd against time and airmass. The "+" indicate observed data points and the solid lines are Beer's law fitting curves. Upper: data from the night on September 5, 1999, demonstrating typical good night, and the standard deviation of the fitting is 0.007, 0.005, 0.007 (from top to bottom). Lower: data from the night on September 17, 1999, demonstrating a typical cloudy night, and the standard deviation of the fitting is 0.219, 0.183, 0.077 (from top to bottom).

4.2. Atmospheric Extinction

To eliminate the effect of the atmospheric extinction, observations are carried out for as long as possible during the night so that a measurement of the intensity at varying airmass can be obtained which should follow the Beer's law:

$$I = I_0 e^{(-\alpha z)}, \tag{17}$$

where I is the observed intensity, α is the atmospheric extinction coefficient, z is the local airmass and I_0 is the intensity at zero airmass – the intensity the would be received if the earth had no atmosphere.

The information about the airmass, z , as determined from the altitude of the moon in the sky at different times (REFERENCE), is incorporated into the airmass fitting to get the fitting parameters α and I_0. Then, the observed intensity at each moment, I_i, is corrected, using the airmass, to the intensity at zero airmass, $I_i^0 = I_i \exp(\alpha z)$. I_0 from the fitting is further used as intensity for that night's lunar phase function.

The goodness of the fit to Beer's offers a ready criterion by which each night's local sky can be judged – the “good” night's data can be separated from the "bad" (noisy) nights. In practice, unless it is cloudy, the data from almost all observable nights are preserved and the standard error in the fitting for each night is further used as the input error for the lunar phase function fit. Figure 3 shows an example of a typical good night and a bad night, as judged by the Beer's law fitting. Experience from the observations shows that the data usually follow Beer's law quite well, and the accuracy of the moonshine fitting is often better than 1%. Among the 171 useful nights we have to date, for 41 nights the accuracy of the fitting is better than 0.5%, for 97 nights better than 1% and better than 2% for the rest of the nights. Beyond atmospheric transmission, earthshine is further influenced by the changing of the earth during a given night, e.g., the sun rising over China. Hence the fitting of the earthshine yields a standard deviation which is, in general, larger than in the moonshine fitting by one-half to one percent. This latter difference contains the signal of the earth's albedo.

5. Lunar Phase Function

The lunar phase function, defined in §2 as the change of moonshine intensity as a function of the phase of the moon, is measured from the readout intensity from each of the fixed fiducial patches used throughout the observations, after carrying out, step-by-step, each of the corrections described above. When the observed intensity read out is plotted against the lunar phase, the data are quite scattered around the average curve (Figure 7a). Most of such scattering is not simply due to unknown or random source of noise, but can be systematically removed. Several steps of calibration are necessary before we have an accurate measurement of the lunar phase function.

5.1. Atmospheric Correction

The measurement of the moonshine intensity on different nights, even after extrapolation to zero airmass, is subject to changes in the local atmospheric conditions. Because of this, there is a deviation in the intensity measured from the same fiducial patch at the same lunar phase on different nights (that is, successive lunar cycles). The standard practice of most of the night observations is to use standard stars to calibrate the night. We have found that the crescent of the moon is our best standard "star". That is, we correct from night-to-night using the correlation between the change of the moonshine intensity and the crescent intensity.

We use a fifth degree weighted polynomial fit for both the fiducial patch intensity and the average crescent intensity over the area of the bright portion as a way to determine the average of the intensity at each lunar phase. Because of the pronounced opposition effect which gives a sharp increase in the moonshine intensity when lunar phase approaches zero degrees (see Figure 1), in the polynomial fitting, twice the weight is given to data points within an angle of +/-5 degrees. The deviation of the measured intensity at each data point from the fitting curve in both the moonshine case and the crescent case are obtained, and the cross correlation between these errors

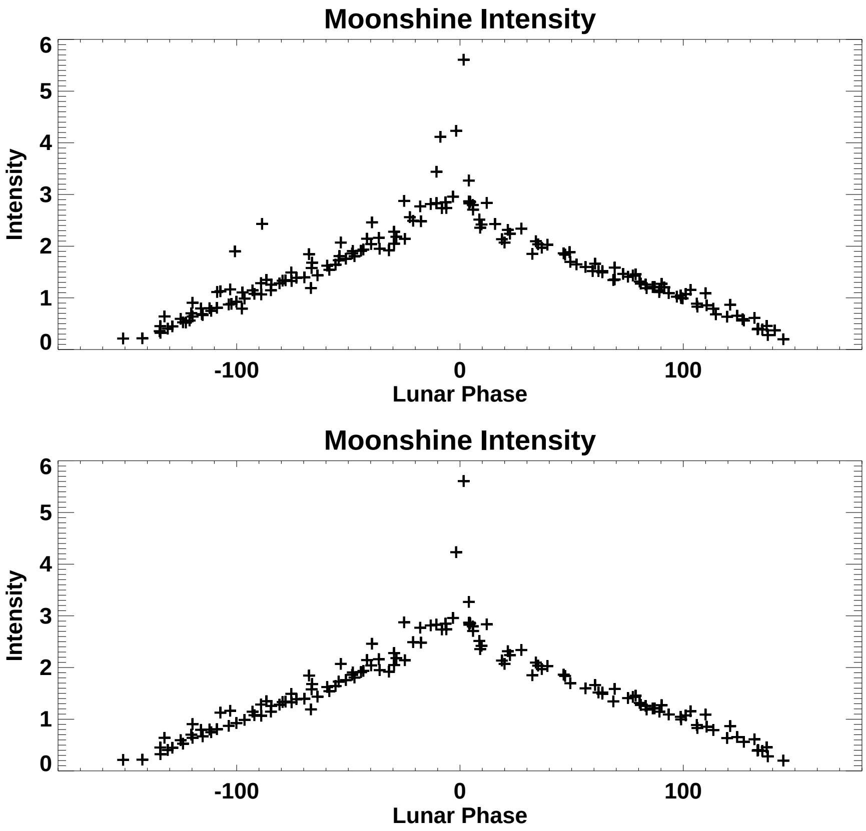

Fig. 4.— The lunar phase function plots from the raw data without correction. Top: from all nights' data; bottom: from data with Beer's law fitting standard deviation less than 0.02.

are calculated. For the morning observations, for which the lunar phase is positive, we get a cross correlation of 0.61, see Figure 5. A simple least-square linear fit is made between the moonshine deviation and crescent deviation (equation 17) and the correlated part of the error is subtracted from the moonshine data as a correction for the nightly variation (equation 18).

$$\frac{I_i - \bar{I}_i}{\bar{I}_i} = a_0 \times \frac{C_i - \bar{C}_i}{\bar{C}_i} + b_0 + S_i \tag{17}$$

$$I_i' = I_i - a_0 \times \bar{I}_i \times \frac{C_i - \bar{C}_i}{\bar{C}_i} \tag{18}$$

Here I_i is the observed fiducial patch intensity, C_i is the crescent intensity, $\bar{I}_i$ and $\bar{C}_i$ are the average fiducial patch intensity and crescent intensity, respectively, at the same lunar phase. The coefficients a_0, b_0 and c_0 are derived from the least square fitting of equation (16). The scattering

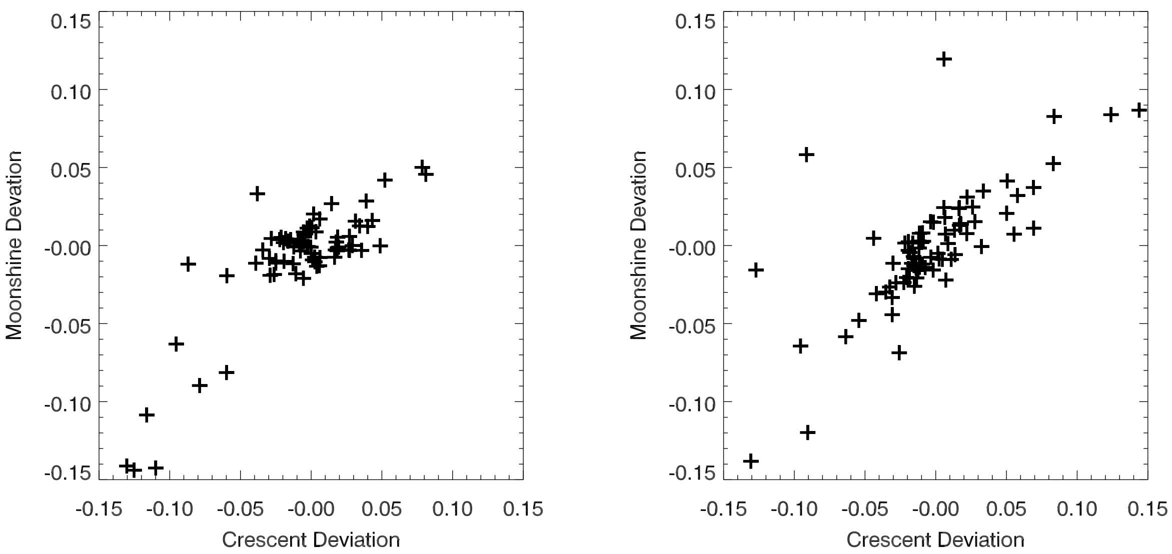

Fig. 5.— The deviation of the moonshine fiducial patch intensity from average against the deviation of the overall intensity of the crescent. Left: data points from morning observation; right: data points from evening observation.

among the datapoints is much reduced after this correction (Figure 7b). This correction is more significant for the evening data (lunar phase ¡ 0) because in the evenings, we are mostly observing the moon in the western sky, over Los Angeles and the Pacific Ocean, which are more subject to local atmospheric changes.

5.2. Declination Correction

The second step correction is made by taking into consideration of the relative position of the moon and the sun with respect to the earth. The difference in right ascension between the sun and the moon (hereafter we call it "relative right ascension") changes from 180 to -180 degree which essentially determines the lunar phase, defined as the angle from between the moon-earth line and the sun-moon line, see Figure 1. The difference in the declination between the sun and the moon (hereafter "relative declination") changes as well, since the orbital plane of the moon around earth is inclined to that of the earth around the sun. Toward the full moon, the relative declination also becomes important in determining the lunar phase. As a result, at the same lunar phase, but on different nights (that is, different months), the position of the moon may be different, and this difference alters the readout intensity of the fiducial patches. To correct for this effect, for a given lunar phase around the full moon, we choose a standard position of the moon, and normalize the readout intensity of different positions to this standard position. The standard position is the one for which the relative declination is zero and the lunar phase is equal to the relative right ascension. The normalization is made as follows:

$$I_i - \bar{I}_i = a_1 P_i + b_1 D_i + c_1 + S_i, \tag{20}$$

where I_i is the observed intensity, $\bar{I}_i$ is the average intensity at the same lunar phase as I_i, obtained from a fifth degree polynomial fitting, P_i is the absolute value of the difference between the lunar phase and the relative right ascension, D_i is the relative declination, a_1, b_1, and c_1 are fitting parameters which are determined from the least square fitting using all the observed intensities. The normalized intensity, I_i', is derived by taking P_i and D_i as zero:

$$I_i' = I_i - (a_1 P_i + b_1 D_i) \tag{21}$$

This correction is only made for lunar phase between -15 and +15 degree since the effect of the relative position of the moon is only important around the full moon. After this correction, the data points which were originally quite noisy around the full moon get tighter (Figure 7b).

5.3. Libration Correction

The third step correction accounts for the lunar libration. Since the orbit of the moon around the earth is not parallel to the equator of the moon, the north pole and south pole of the moon are seen alternatively during each orbit. This is latitudinal libration. Since the orbit of the moon is not a circle but slightly elliptic, the moon moves faster at apogee than at perigee, hence the

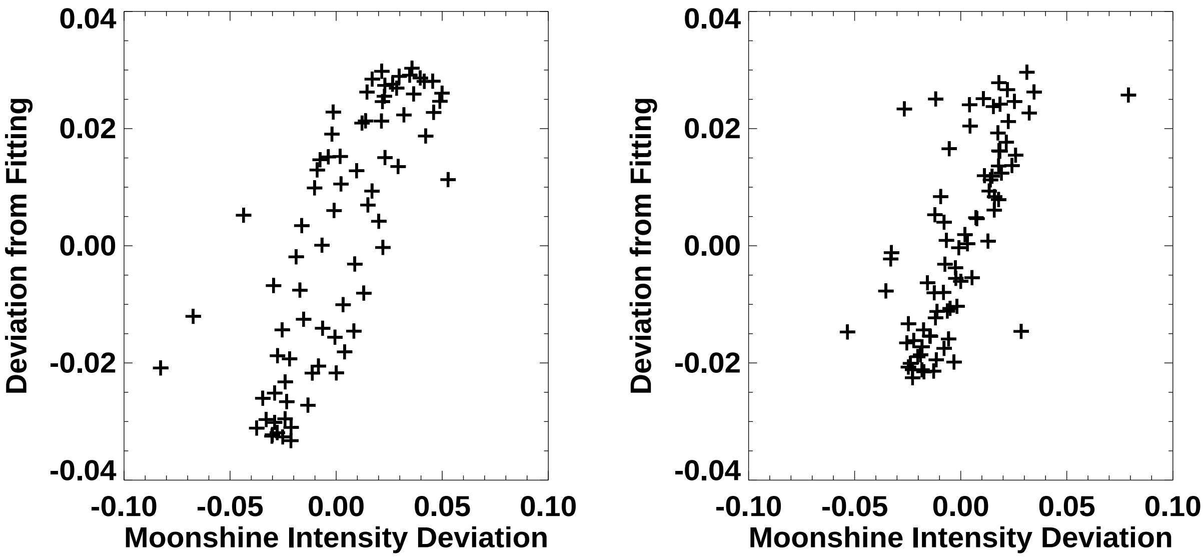

Fig. 6.— The deviation of the moonshine fiducial patch intensity (after the first and second step correction) from average against the deviation as a fitting result from Equation 6. Left: data points from morning observation; right: data points from evening observation.

moon is seen wobbling around its axis of rotation – this is its longitudinal libration. As a result of both kinds of libration, in different cycles of the lunar orbit, even at the same lunar phase, we would expect a change in the positions of the fiducial patches on the lunar disk. The read out intensity, thus changes as a function of the geometric postion of the fiducial patch on the lunar disk. Specifically, the longitudinal and latitudinal librations, have the consequence that, at the same lunar phase, there are multiple values of moonshine intensities for a given lunar phase. To first order accuracy, we derived a description of the deviation of the observed intensity to the averaged intensity, as a linear function of the longitudinal and latitudinal librations, which goes as:

$$I_i - \bar{I}_i = a_2 L_i^\alpha + b_2 L_i^\beta + c_2 + S_i \tag{22}$$

Where L_i^α is the longitudinal libration, and L_i^β is the latitudinal libration. The coefficients a_2, b_2 and c_2 are obtained from the least-square fit of the above equation. We, then, correct the intensities by subtracting the calculated deviations to remove the effect of libration (figure 5d). The principle of this operation is the same as in step 2.

The lunar phase function for both fiducial patches are produced with from a fifth degree weighted polynomial fit to the corrected data. The same algorithm is used for all the steps above as the means of deriving the average of the intensities through the lunar phase. After each step of correction, the standard deviation of the fit is deduced from orginally 0.07/0.04 (evening/morning) to 0.04/0.03, 0.02/0.02, and eventually 0.01/0.01 with the phase function normalized to unity. A restricted regularized fitting is performed, as well which parameterizes the intensities at 181 bins(corresponding to lunar phase 0 to 180 degree). These 181 parameters from the fitting describe the lunar phase function in that the intensity of any lunar phase is the linear interpolation between the values at the two grids in which the lunar phase falls in.

6. Determination of the Albedo

The effective albedo is calculated from the earthshine measurement from combining equations (8) and (16):

$$A^* = \frac{3}{2}\frac{f_b}{f_L}\frac{I_a}{I_b}\frac{R_{em}^2}{R_e^2}\frac{p_b}{p_a}, \tag{23}$$

where I_a/I_b is the ratio of the earthshine intensity to the moonshine intensity; I_a and I_b are both the extrapolated intensity to the zero airmass, corrected with the transmissions of the filters, flatfielding, background subtraction, and change of the lunar radius in the image plane. The ratio between the physical reflectivity of the two fiducial patches, $\frac{p_b}{p_a}$, is determined from the lunar eclipse data taken at BBSO on November 29, 1993. The lunar phase function for the bright side, f_b, is used in the formula to account for the geometrical dependence of the reflectivity of the moon.

For convenience, the measured earth's albedo is often expressed as the magnitude of the effective albedo, A^* (see equation 8), i.e.,

$$[A^*] = -2.5 log A^* \tag{23}$$

So far, observational data have been accumulated for 11 months covering the winter of 1998-1999

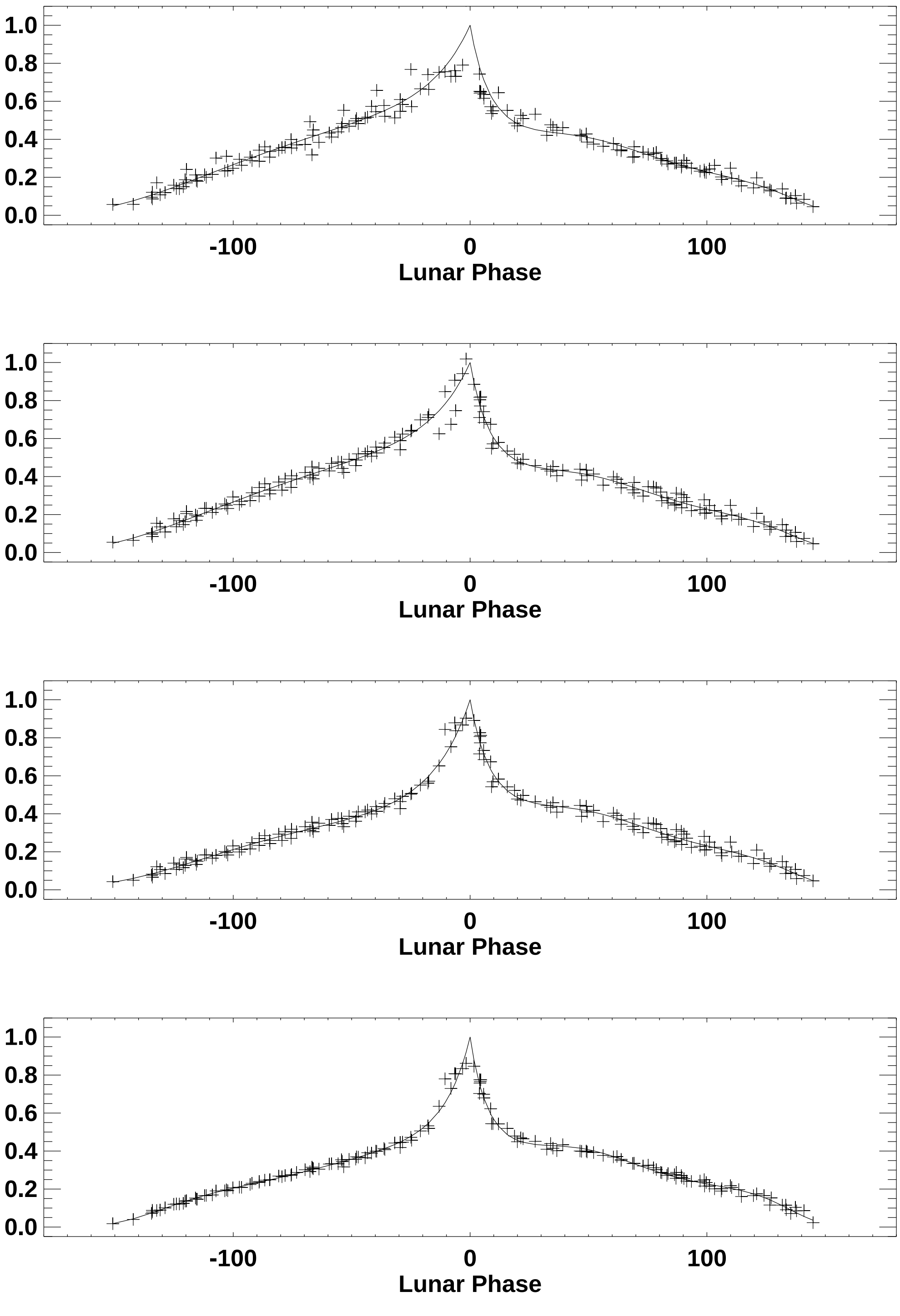

Fig. 7.— Lunar phase function plots from the raw data and from data after each step of correction.

through the fall of 1999. Both the instantaneous [A*] variation during each single night and the variation of the nightly average [A*] throughout the seasons have been obtained and compared to the simulated results using a scene model and satellite cloud cover data.

6.1. Image Analysis

7. Modelling

8. Conclusions

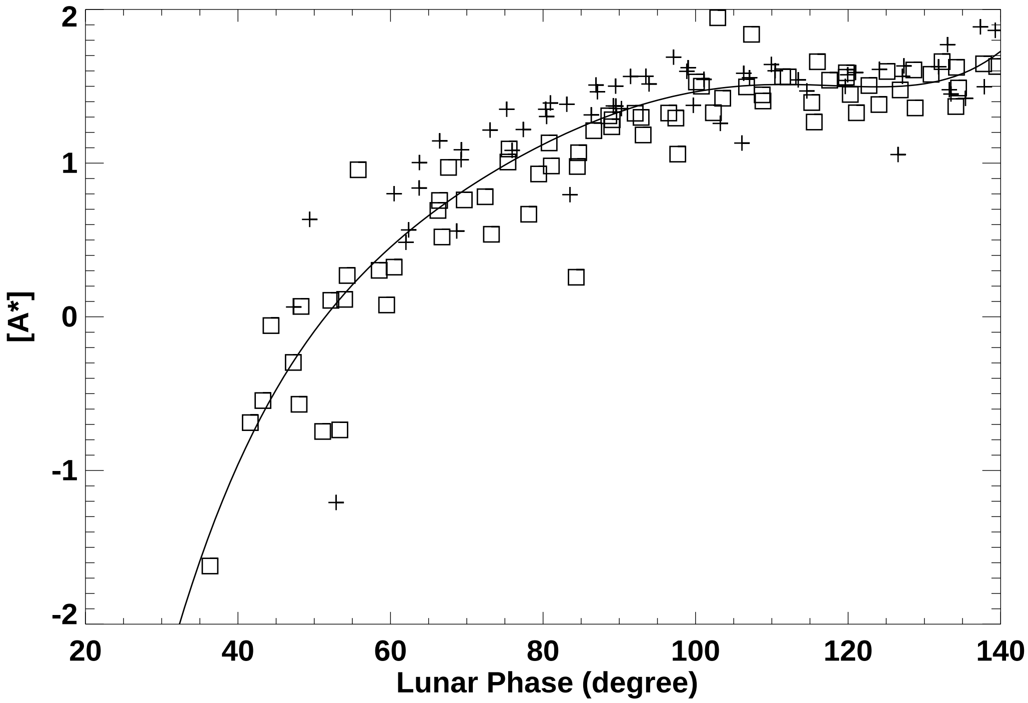

Fig. 8.— Plot of [A*] (see equation 23) from all observing nights against lunar phase (in absoluate value). Each data point represents the averaged [A*] value throughout one night; "plus" indicates morning observation (lunar phase > 0) and "square" indicates evening observation (lunar phase $<$ 0). The solid curve is a 5^{th} degree polynomial fit of the data points.

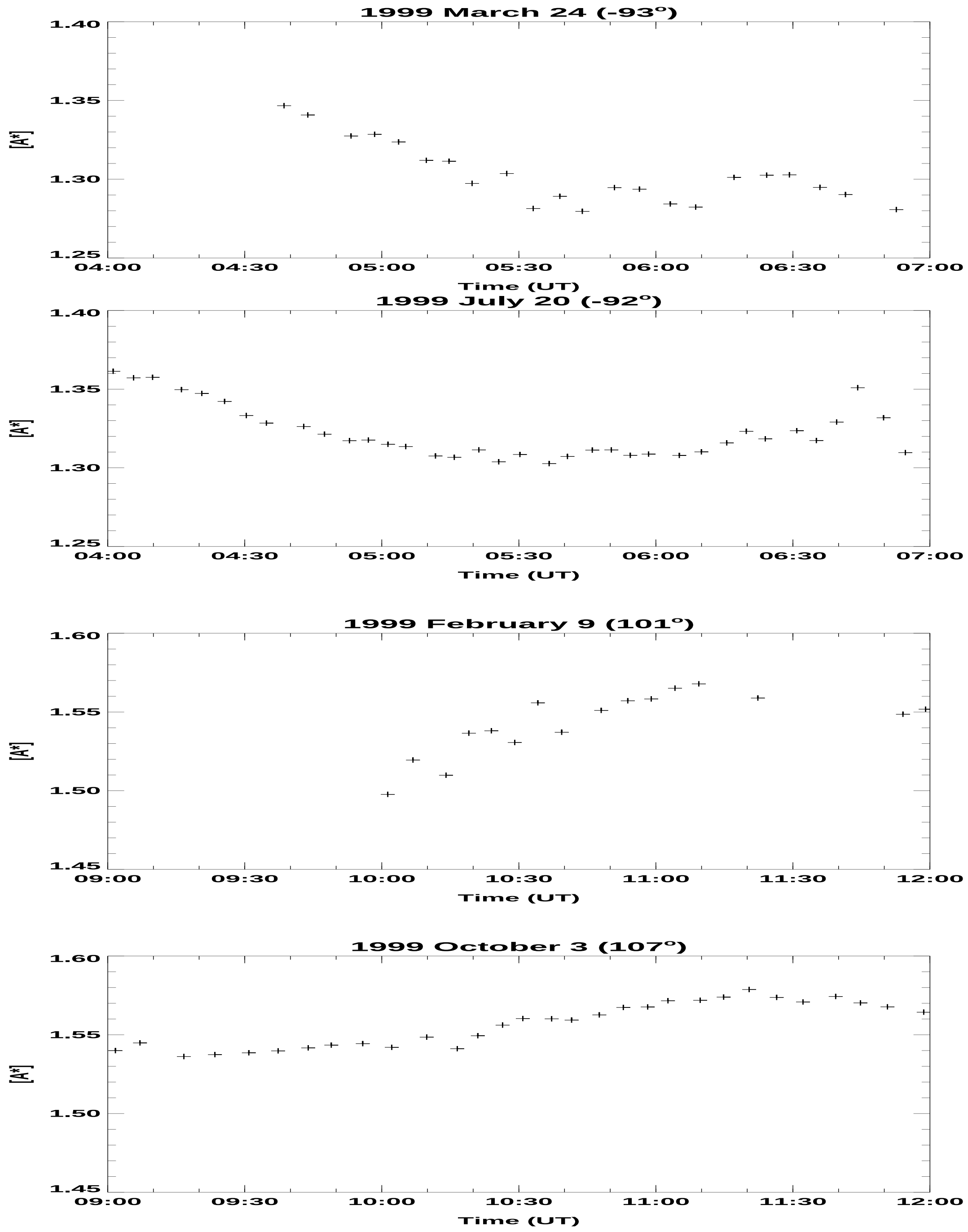

Fig. 9.— Plots of [A*] observed in the night of (a) 1999 March 24, (b) 1999 July 20, (c) 1999 February 9, and (d) 1999 October 3 against the time of observations.

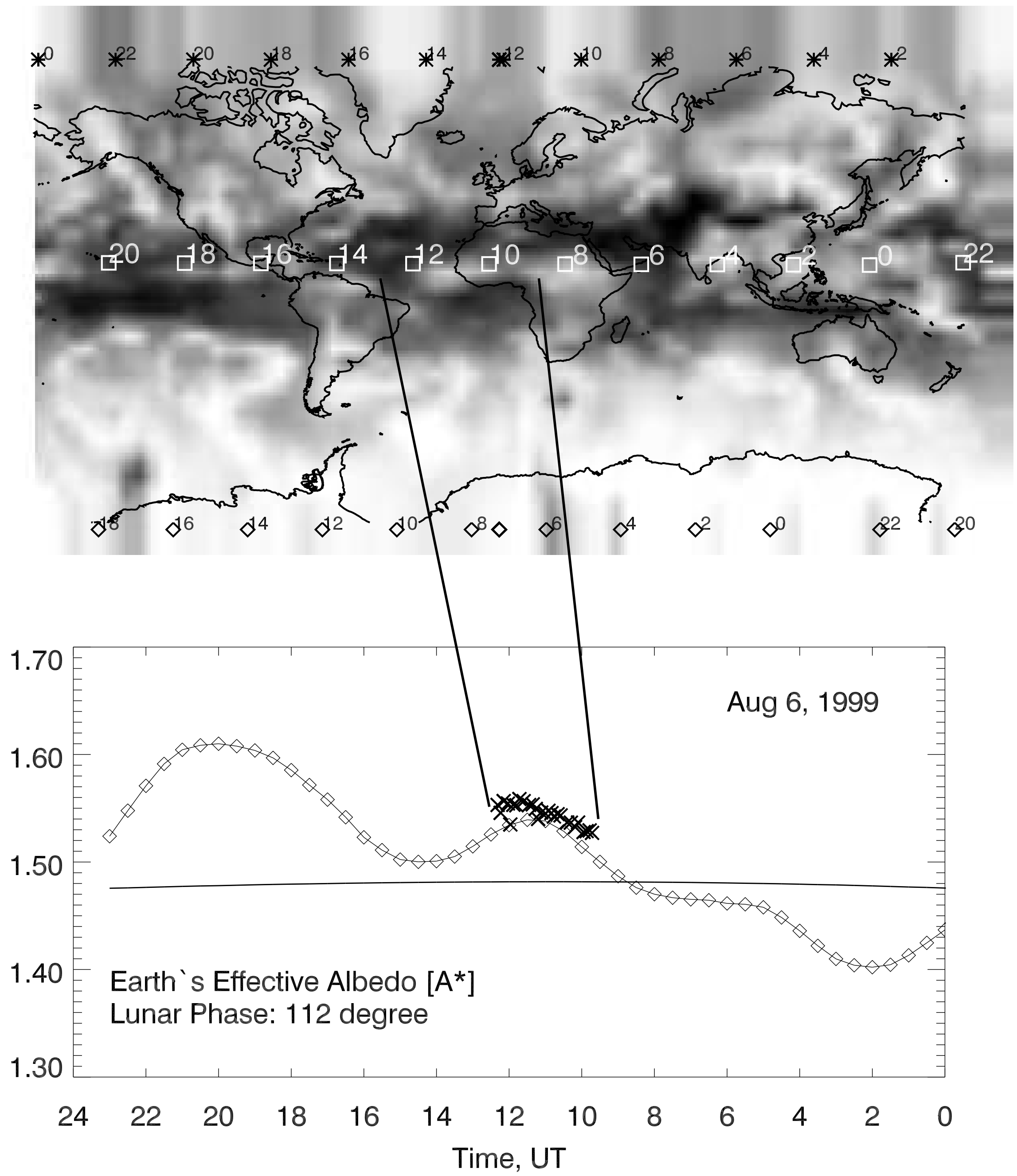

Fig. 10.— August 6th

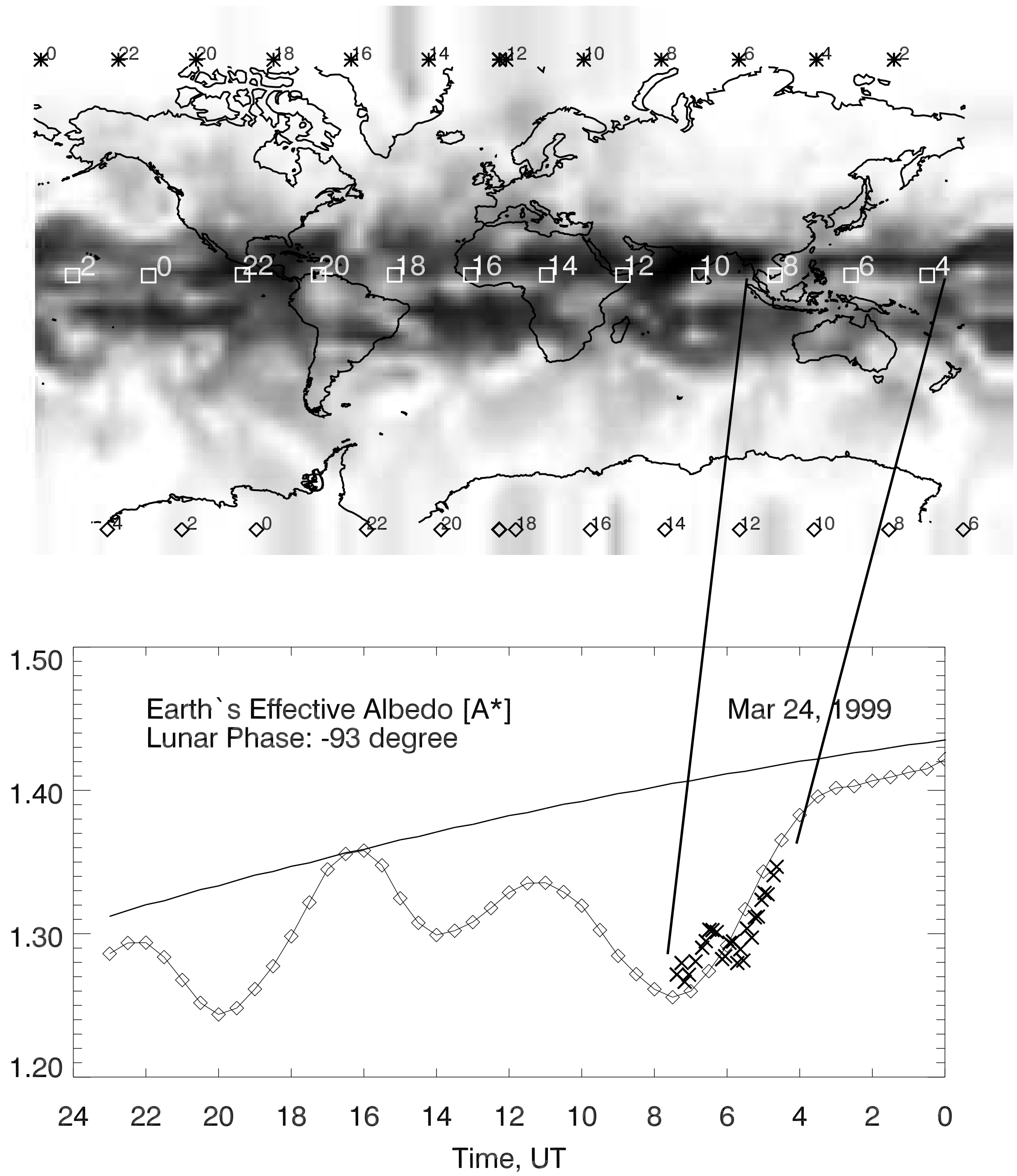

Fig. 11.— March 24th

REFERENCES

Danjon, A., 1928, Ann. Obs. Strasbourg, 2, 165

Danjon, A., 1954, in The Earth as a Planet, ed. Kuiper, p.726, Chicago

Dubois, J., 1947, Bull. Astron., 13, 193

Franklin, F.A., 1967, J.Geophys.Res., 72, 2963

Huffman, D., Weidman, C. and Twomey, S., 1990, Colloq Andre Danjon, Jounees 1990, Capitaine and Detarbat, eds. (Paris: Paris Observatory), p. 111

Kennedy, J.R., 1969, M.S. Thesis, Fresno State College, unpublished

Rougier, M., 1933, Ann. Obs. Strasbourg, 2, Part 3, 203

Svensmark, H. and Friis-Christensen, E., 1997, J. of Atm. and Solar-Terrest. Physics, 59, 1225.

Very, F., 1915, Astron.Nach., 201, 353

This manuscript was prepared with the AAS LaTeX macros v4.0.